Numerical prediction of the decline of the shale gas production rate with considering the geomechanical effects based on the two-part Hooke's model

Jiangtao Zheng [a,b], Yang Ju [a,c,⇑], Hui-Hai Liu [d], Liange Zheng [e], Moran Wang [b]

[a] State Key Laboratory of Coal Resources and Safe Mining, China University of Mining & Technology at Beijing, Beijing 100083, China
[b] Department of Engineering Mechanics, School of Aerospace, Tsinghua University, Beijing 100084, China
[c] State Key Laboratory for Geomechanics and Deep Underground Engineering, China University of Mining & Technology, # 1 University Avenue, Xuzhou 221006, China
[d] Aramco Research Center, Houston, TX 77084, USA
[e] Earth Sciences Division, Lawrence Berkeley National Laboratory, Berkeley, CA 94720, USA

a r t i c l e i n f o

Article history:
Received 14 February 2016
Received in revised form 24 April 2016 Accepted 28 July 2016
Available online 6 August 2016

Keywords:
Shale gas
Production rate decline Two-part Hooke's model
Stress-sensitive permeability Numerical estimation

a b s t r a c t

The production rate of a typical shale gas well generally has steep decline trend at the initial stage but small declines at later times. Some empirical relationships have been proposed to describe the declining production rates and thus forecast the final cumulative production of a shale gas well. However, these empirical relationships can hardly elucidate the mechanisms that cause the special shale gas production trend. In this study, a novel two-part Hooke's model (TPHM) for the permeability and effective stress relationship is developed and incorporated into the hydro-mechanical COMSOL solver to determine the pro- duction rate of shale gas wells against time. The TPHM conceptualizes shale rock into soft part and hard part, which comply with the natural-strain-based and engineering-strain-based Hooke's laws, respec- tively, and contribute differently to the decreasing permeability with increasing effective stresses. The simulation results are analyzed and compared with those for which the permeability change effect is not considered. The analysis indicates that the decrease in stress-induced permeability plays a non- negligible part in the decline of the production rate.

1. Introduction

Shale gas, as a valuable natural gas, has recently drawn great international interest following the boom of the shale gas indus- tries in the United States [1,2]. As an unconventional gas resource, the economical extraction of shale gas hinges on effective treat- ment of the extremely low-permeability shale layer (usually on the magnitude of nano-Darcy) using horizontal drilling and hydraulic fracturing technology [2]. One of the distinct characteris- tics of the shale gas production rate is that it declines sharply in the initial stage with a long tail in the later stage. The sharply decline trend has raised skepticism about the estimated ultimate recoveries (EUR) and the overall economic feasibility of shale gas plays [3]. Therefore, accurate knowledge about the production decline curve for the basis of estimating the EUR is fundamentally important. For other reasons, comparative studies on the production decline curve among different production wells, different geological conditions and different production techniques may lead to optimal methods for increasing shale gas production.

Conventionally, the prediction of the production decline curve for shale gas wells is based on the data collected from previous production wells or empirical relationships because these methods provide a quick estimation. The Arp's equation [4], which was initially derived for conventional wells, is employed to predict shale gas well production rates as well. The Arp's equation can be written as:

$$Q(t) = \frac{Q_i}{(1 + bDt)^{1/b}} \quad (1)$$

where $Q(t)$ is the production rate at time t, Q_i is the initial production rate, and b and D are empirical parameters that are estimated from similar wells. However, Arp's equation is not used without question [5]. Many researchers [5–7] have attempted to modify Arp's equation for better describing the production decline curve of shale gas wells. These predictions provide an initial understanding of the shale gas production rate but with little consideration of the shale gas flow mechanisms.

⇑ Corresponding author at: State Key Laboratory of Coal Resources & Safe Mining, State Key Laboratory for Geomechanics & Deep Underground Engineering, China University of Mining & Technology, D11 Xueyuan Road, Beijing 100083, China.
E-mail addresses: yju@icloud.com, juy@cumtb.edu.cn (Y. Ju).

http://dx.doi.org/10.1016/j.fuel.2016.07.112

Nomenclature

a	material constant of the soft part (m^2)
b	material constant for the hard part (dimensionless)
$/_e$	hard part porosity (dimensionless)
$/_t$	soft part porosity (dimensionless)
c_t	soft part proportion (dimensionless)
r	effective stress (MPa)
C_e	compressibility of the hard part porosity (MPa^{-1})
k_e	hard part permeability (m^2)
k_t	soft part permeability (m^2)
K_t	elastic modulus of the soft part (MPa)
m	material constant of the soft part (dimensionless)

Unit conversion
Pressure SI unit: 10^6 Pa; Field unit: 145.04 psi
Production rate SI unit: 10^4 m^3/Day; Field unit: 355 MSCF/Day

For a better evaluation of the shale gas production rate, a num- ber of reservoir modelling method has been proposed with more concerns about the inherent gas transport mechanisms in nano- pores [8–13], gas adsorption and desorption effect [1,14,15], two phase flows effect [16,17], multiscale transport phenomenon [18–20], influence of inner porous structure and composition of shale [21], different type of fracturing fluid [22,23] and geome- chanical effect [24–27]. Among these influences, the geomechani- cal effects play an important role in the reduction of production rate [26,28–30], especially in the early stage of the production. Along with the production, the reservoir pressure decrease and effective stress increase which leads to the value changes of many mechanical and hydraulic properties of the shale layer [28]. It has been widely reported that the permeability, which is fundamental to the production rate prediction, showed a high sensitivity to the changes in effective stress [30–35]. Specifically, permeability of a shale rock usually decreases rapidly (usually larger than one order) within the low effective stress range and then decrease relatively slow at high effective stress range [31,36]. However, in the previ- ous studies [37–39] constant permeability or empirical relation- ships between permeability and effective stress, which cannot accurately characterize the permeability changes at the whole stress range, were usually employed in the reservoir models for the prediction of shale gas production. Therefore, a physically robust relationship between permeability and effective stress in a wider stress range is in need for the accurate characterization of a shale gas well.

In this work, a more physically robust relationship between permeability and effective stress is proposed and incorporated in the shale gas production simulation. Specifically, a newly devel-

The rest of the paper is organized as follows: in Section 2, the concept of TPHM and the derivation of stress dependent perme- (http:// www.comsol.com/) for the simulation of shale gas production. For the sake of the manageability of the study, the desorption effect, two phase flow influences, thermal effect and chemical reac- tions are not included in the simulation. This leads to difficulties to compare our prediction results with those of field cases that involve the above processes. Nonetheless, numerous investigations indicate that the change of stress state significantly modifies the permeability of shale rocks [30–35]. Considering this fact, a simu- lation procedure, which can accurately take into account the per- meability changing effects along with the production, is imperative for the shale gas reservoir modelling. In this study, the effect of shale matrix permeability changing along with the

ability relationship are presented. In Section 3, the model con- structed in COMSOL is introduced. In Section 4, the simulation results are displayed, and the importance of including geomechan- ical effects in shale gas production simulation is discussed. Con- cluding remarks are made in Section 5.

2. Relationship between permeability and effective stress

Reservoir rock permeability is one of the most important prop- erties for predicting the shale gas production rate. Shale gas reser- voirs usually have extremely low permeability [1,26,28], and abnormally high pore pressure which is formed either by diagene- sis or by hydrocarbon-generation [40–42]. It is understandable that the reservoir pore pressure decreases along with the produc- tion while the overburden pressure or confining pressure almost remains constant. This results in the increase in effective stress according to the Terzaghi effective stress calculation theory [43,44]. Considering that the reservoir permeability is highly stress sensitive and is directly related to the gas production rate, it is imperative to include this geomechanical effect in the shale gas production prediction model. The relationship between permeabil- ity and effective stress used in our model is based on the TPHM proposed by Liu et al. [36,45–47].

2.1. A brief introduction to the TPHM

Liu et al. [36,45–48] suggested that the *true strain* or *natural strain*, rather than the *engineering strain*, should be used in Hooke's law for accurately modelling elastic deformation of rock, unless the two strains are essentially identical (as they might be for infinites- imal mechanical deformations). Natural rocks are inherently heterogeneous [49,50] which means different varieties of Hooke's law should be applied within ranges having significantly different stress–strain behavior. Liu et al. [46] conceptually divides the rock body into two parts, hard and soft, and hypothesizes that the soft part obeys the natural-strain-based Hooke's law, whereas the hard part approximately follows the engineering-strain based Hooke's law for mathematical convenience. With this conceptually divid- ing, a number of constitutive relationships between stress and rock mechanical and hydraulic properties can be reasonably derived by using a consistent set of parameters with clear physical meaning [45,46]. Its validity is demonstrated by its consistence with a num- ber of test data [36,45–47].

The TPHM based porosity–stress relationship under a hydro- static state can be expressed by [46]:

$$\phi = \phi_{e,0}(1 - C_e\sigma) + C_t \exp\left(-\frac{\sigma}{K_t}\right) \quad (2)$$

which involving more complete physical processes characteriza- tion, can be carried out provided that more accurate information of reservoirs is available.

$$\phi_e = \phi_{e,0}(1 - C_e\sigma) \quad (3)$$

$$\phi_t = C_t \exp\left(-\frac{\sigma}{K_t}\right) \quad (4)$$

Hereafter, subscript e denotes the "hard part", t refers to the "soft part", and 0 refers to the unstressed state. ϕ is porosity and σ is effective stress which is defined as the confining stress minus the pore pressure. C_e is the compressibility of the "hard part", K_t is the bulk modulus of the "soft part" and C_t is the proportion of the "soft part". Usually, the soft part accounts for only a small portion in the conceptualized model. As noted by Liu et al. [36,45,46], the soft part refers to some portion of the pores and micro-cracks in a rock body, which could be subjected to significant deformation due to their geometrical heterogeneity [51–54]. Under this conceptu- ally divided framework, the rock behavior with applied stress can be more accurately described.

It should also be noted that the TPHM is a macroscopic model that deals with mechanisms of micro-mechanics in a phenomenol- ogy manner. As a result, the parameters in the TPHM based rela- tionships are determined from the macroscopic experimental data. A typical laboratory tested porosity–effective stress data [31] is shown in Fig. 1, as indicated by little black squares. Accord- ing to the tendency of the experimental data of porosity against effect stress, determination of the unknown parameters in Eq. (2), i.e. $\phi_{e,0}$, C_e, C_t, K_t, can be divided into two steps. First, the parameters of the "hard part" are determined. Considering the clo- sure effect of micro-cracks under a high effective stress roughly ranging within 35–120 MPa, the influence of the "soft part" on the changes of porosity can be ignored. Therefore, the hard part porosity relationship $\phi_e = \phi_{e,0}(1 - C_e\sigma)$ is adopted to match the porosity–effective stress data at this range, as indicated by the red straight dash line in the figure, from which, $\phi_{e,0}$, C_e can be determined. Secondly, the parameters of the "soft part" are deter- mined considering the contribution of micro-cracks to the change of porosity at a low effective stress roughly ranging within 0–15 MPa. The value of C_t can be determined by $\phi_0 - \phi_{e,0}$ at

$r = 0$, if the ϕ_0 is provided from the experiment. Otherwise, ϕ_t is first obtained by using the laboratory test data ϕ minus the already obtained ϕ_e value at relatively low effective stress level. Then, fitting the data of ϕ_t and r using the equation $\phi_t = c_t \exp$ gives the values of c_t and K_t. The contributions of soft part porosity and hard part porosity are indicated by black shadow and red shadow in the Fig. 1, respectively.

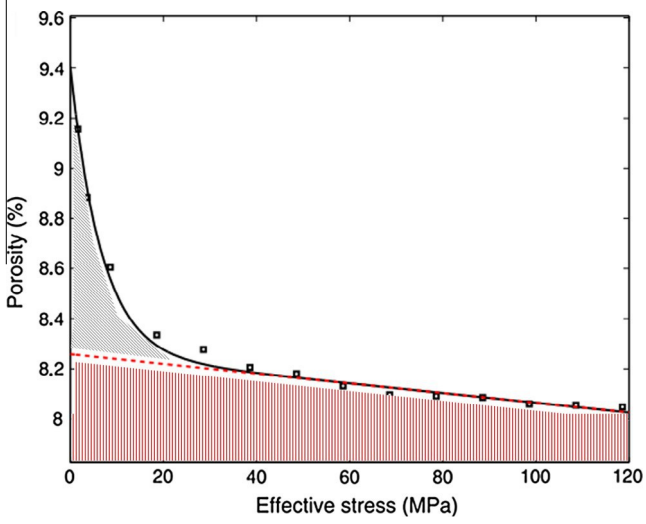

2.2. Stress-dependent rock permeability

It is conceivable that the rock permeability decreases with increasing effective stress in the elastic stage because of the com- paction of pore volume, i.e. transport channels. One particular phe- nomenon for low-permeability rock is that the permeability decreases rapidly (up to several orders) along with the first several megapascal effective stress increases. As demonstrated by many experimental studies, this rapid decrease in permeability is the result of micro-cracks closure [36,55–58]. However, most existing models cannot accurately describe the permeability–effective stress relationship mainly because they consider rock as a homoge- neous material. In contrast, the TPHM considers the heterogeneity of natural rock and can more accurately describe the relationship between permeability and effective stress.

According with the division of porosity into ‘‘hard part” and ‘‘soft part”, one can consider the contribution of these two parts to permeability respectively. First, the permeability changes in rel- atively high effective stress range are dominated by the hard part with the consideration that the soft part can be neglected in this stress range due to micro-cracks closure. Mathematically, the stress-dependent hard part permeability can be empirically given by an exponential law (as shown in Eq. (5)), which is consistent with most of the experimental observations [6,10,23,24] at relatively high effective stress range. Secondly, the soft part corresponding to those slot-like micro-cracks according to the division of the porosity. The flow in crack-shape channels or two parallel plates is governed by the well-known ‘‘cubic law” [53,59,60]. For a given rock volume, whose flow space can be conceptualized as crack-shape flow channels, the permeability is related with the aperture of cracks by the cubic law. Meanwhile, the porosity is lin- early correlated with the aperture of cracks. Thus, the soft part per- meability change with the soft part porosity should obey a power law similar with the ‘‘cubic law” [32,59,60] (as shown in Eq. (6)). In other words, the value of m value should be near 3. This has been verified in our previous work [36] using the experimental data pro- vided by Dong et al. [31]. Combining Eqs. (5) and (6) yields the total stress-dependent permeability as Eq. (7).

$$k_e = k_{e;0}\exp\left[b(\phi_e - \phi_{e;0})\right] = k_{e;0}\exp\left[-bC_e\phi_{e;0}r\right] \quad (5)$$

$$k_t = a\phi_t = a\,c_t\exp\left[-\frac{r}{K_t}\right]^m$$

$$k = k_{e;0}\exp\left[-bC_e\phi_{e;0}r\right] + a\,c_t\exp\left[-\left(\frac{r}{K_t}\right)^m\right] \quad (6)$$

(7)

Fig. 1. Relationship between porosity and effective stress. The black and red parts

where k_e, k_t are the stress-dependent permeability of the hard part and soft part, respectively; the combined term $bC_{e,0}$ for the hard part has similar meaning with the stress sensitive coefficient in an commonly used empirical exponential law for describing the stress dependent permeability; b is a material constant of the hard part; a and m are material constants of the soft part.

A typical laboratory tested permeability–effective stress data [31] is shown in Fig. 2, as indicated by little black squares. Note that the permeability is plotted in logarithmic coordinates. Determina- tion the value of $k_{e,0}$, b, a, m is similar with the two-step procedure described in the Section 2.1. First, the permeability data at relatively high effective stress range are matched by $k_e = k_{e,0}\exp(-bC_{e,0}r)$ to determine the values of $k_{e,0}$ and b. Secondly, k_t is first obtained by using the laboratory test data k minus the already obtained k_e value at relatively low effective stress range. Then, fitting the data of k_t and r using the equation $k_t = a_t \left[\exp\left(-\frac{r}{K}\right)\right]^m$ gives the values of a and m. In our previous work [36], the procedure described above was employed to determine the unknown paramet

tation of the references to color in this figure legend, the reader is referred to the web version of this article.)

(7)

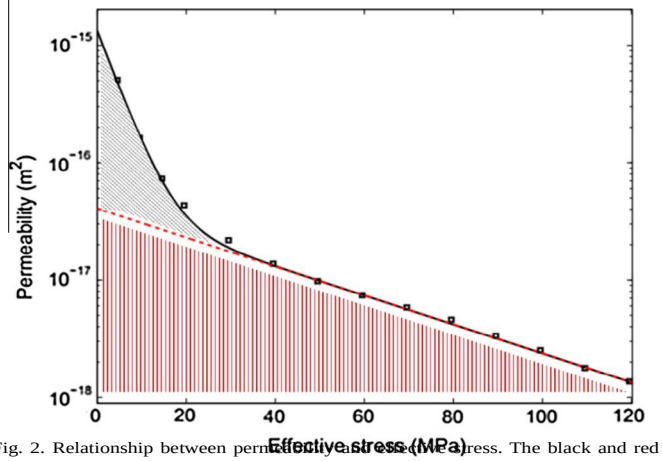

Fig. 2. Relationship between permeability and effective stress. The black and red parts denote the contribution of the soft part and hard part, respectively. (For interpretation of the references to color in this figure legend, the reader is referred to the web version of this article.)

using the experimental data of four groups of shale samples [31]. The determined parameters values are also the basis of the settings in the numerical simulation.

3. Methodology

The COMSOL software was employed to simulate the gas pro- duction process in a simplified shale gas reservoir model. The derived permeability–effective stress relationship of shale matrix was incorporated into the solver to study this geomechanical effect on shale gas production. The geometrical model constructed in COMSOL was simplified, and the stress dependent permeability effects was the focus of the simulation.

3.1. Simplified geometrical model in COMSOL

For the sake of simplicity, the production shale layer is hypoth- esized as blocks, which are segmented by hydraulic fractures and horizontal well, as shown in the upper part of Fig. 3. The reservoir depth is set as 1500 m. The formation thickness is 90 m, the length accessed by the horizontal well is 1000 m, and the half width accessed by the hydraulic fractures (perpendicular to the paper as shown in Fig. 3) is assumed to be 84 m. The distance between hydraulic fractures is 50 m. Under these settings, the size of each block is 50 45 84 m^3, and a total of 80 blocks are ×× ×d by this horizontal well. For the simplicity of the simulation, only one block is take into consideration with the hypothesis that each block has the same contribution to the production. Shale gas is assumed to transport freely to the well head once it flows out of the shale matrix, considering the fact that the effective permeabil- ity of hydraulic fractures and wells are usually several orders higher than that of shale matrices [25]. Thus, only the process that shale gas flows out of the shale matrix is considered in this work. Moreover, the flow velocity is assumed to be uniform along the fracture width (perpendicular to the paper). With these simplifica- tion and assumption, only a 2D rectangle (size: 50 m 45 m) block, is constructed and ×ieshed using the build-in meshing mod- ule in the COMSOL, as shown in the lower part of Fig. 3.

3.2. The physical condition setting in COMSOL

The 2D time-dependent *Porous Media and Subsurface Flow* mod- ule in COMSOL is employed to simulate the production in a shale gas reservoir. The reservoir overburden pressure gradient was assumed to be 23 MPa/km along depth, which led to a confining pressure of the reservoir at 34.5 MPa. The reservoir was assumed as an overpressure reservoir and the initial reservoir pore pressure was assumed to be 30 MPa. In the simulation, the confining pres- sure was assumed as a constant and the pore pressure was consid- ered to decrease with the process of gas production. The effective stress was determined using the confining pressure minus the pore pressure. Besides, the pressure in the production well was assumed to be a constant of 10 MPa. Accordingly, the left and right bound- aries of the block, which were treated as the interfaces between shale matrix and hydraulic fractures, were considered as the flow out boundaries for gas at a constant pressure of 10 MPa. The top and bottom boundaries of the block are set as ‘‘no flow” boundaries.

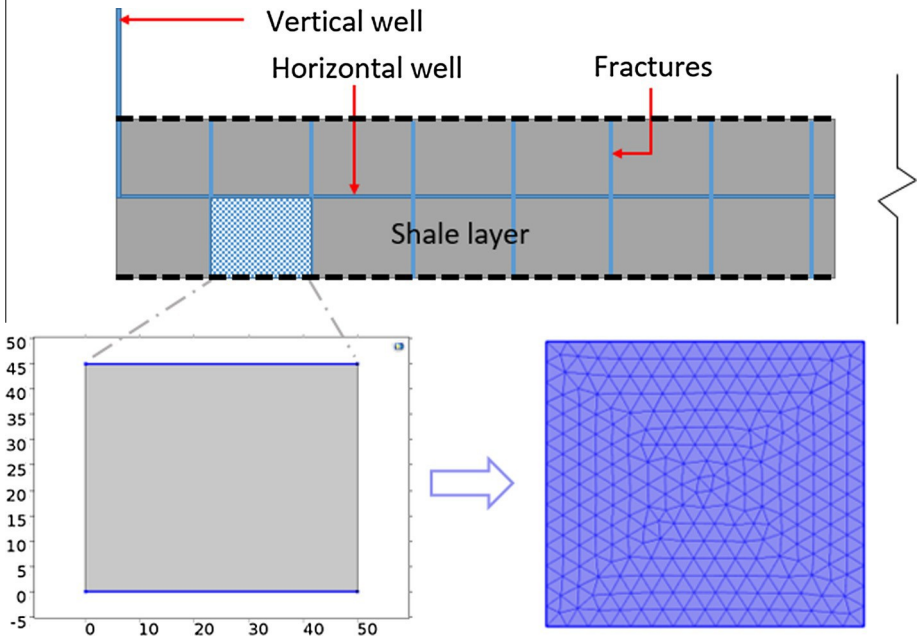

Fig. 3. Simplified geometrical model.

Table 1
Input parameters for shale gas production simulation.

Viscosity (Pa-s)	1.12×10^{-5}

ity are also presented which highlight the importance of considering geomechanical effects.

Permeability (m^2) $k \frac{1}{4}$ $_{e;0}$ – $_{e\,e;0}$ Þ $_{t}$ – k exp $bC \nearrow r$ $a$hc exp($\frac{r}{\lambda i_m}$

$k_{e,0}$ (m^2)	10^{-20}
$bC_e \nearrow_{e,0}$ (MPa^{-1})	0.01
a (m^2)	10^{-16}
C_t	0.005
K_t (MPa)	8.00
m	3.00
Initial pore pressure (MPa)	30.00
Confining pressure (MPa)	34.50
Production well pressure (MPa)	10.00

In contrast to previous studies, the effect of permeability changes along with the effective stress, as presented in Eq. (7), was studied in the simulation. COMSOL provide a very convenient way to set the material parameters as a function of variables. By this way, stress-dependent permeability equation was incorporated into the calculation and updated at each time step. Darcy's law was applied to describe the process of gas flow out of the reser- voir block. Moreover, the shale gas in the production process was assumed to be ideal gas. Table 1 shows the material parameters used in the simulation, the value of which are set according to our previous study [36]. The pressure condition of the reservoir is also provided in this table. Given these settings, time-dependent calculation was performed in the COMSOL.

4. Results and discussion

With the help of the COMSOL software, the reservoir pressure contour, gas flow velocity, and production rates can be calculated. Comparisons with the model that uses constant matrix permeabil-

In this part, some calculation results are shown under the framework settings in Section 3. The reservoir pressure distributions are shown in Fig. 4 at different production times. As displayed, after 5 days of production, the pressure change occurs only near the two flow-out boundaries. Along with the production, the reservoir pressure near the flow-out boundaries gradually become equal to the well pressure, and the overall pressure in the block slowly decreases. Even after 10 years of

4.1. Results of considering permeability change with effective stress

ch higher than the well pressure (16.70 MPa compared with 10 MPa). This suggests that denser hydraulic fractures could be applied to access more gas in the reservoir.

From the calculation, the gas velocity is obtained at each point of the flow out boundary. By integrating the velocity in the flow out boundary and multiplying it by the fracture width and fracture face number, the total flow rates of the reservoir are obtained. Note that this flow rate is at 10 MPa, so we transfer it to the wellhead production rate (at atmospheric pressure) through the ideal gas assumption. The production rate variations in the time range of 1 year and 10 years are shown in Fig. 5(a) and (b), respectively. As shown, the production rate declines rapidly in the first several days, mainly because of the pore pressure decrease near the flow out boundaries. It should be noted that the geomechanical effect plays an important part in this process. Along with production, the gas pressure near the flow out boundaries decrease to the well pressure (recall Fig. 4), which lead to increased effective stress and thus causes the permeability in these regions to decrease rapidly. In the next section, this effect will be analyzed in more detail in

Fig. 4. Reservoir pressure distribution. (a) after 5 days of production, (b) after 1 month of production, (c) after 6 months of production, (d) after 1 year of production, (e) after 5 years of production, and (f) after 10 years of production.

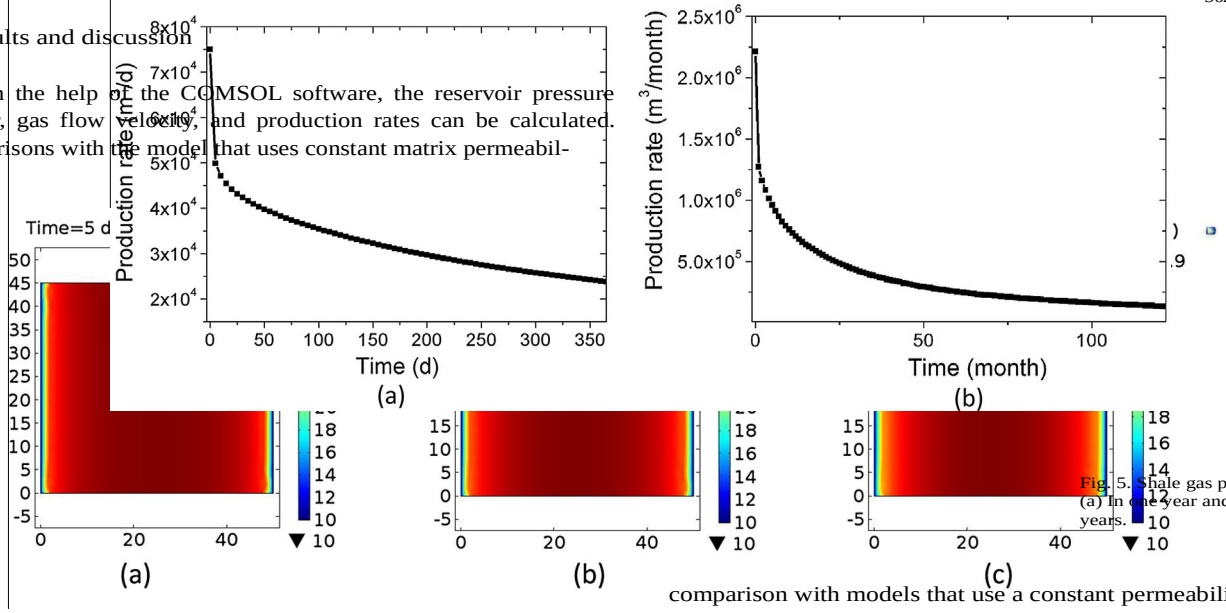

Fig. 5. Shale gas production rate. (a) In one year and (b) in ten years.

comparison with models that use a constant permeability parameter.

4.2. Comparison to the model without considering the geomechanical effect

In this part, the calculated production rate data were compared with the results obtained from the model that has exactly the same settings except permeability. The permeability in this model is set as a constant with the value calculated by Eq. (7) at the effective stress of 24.5 MPa. Fig. 6 shows the comparison result. It is found that the reservoir pressure drop along with the production is the main reason for the decline in the shale gas production rate. However, some major differences can be found between the two models. As shown, the production rate of the constant permeability model has a more gradually declining trend. The

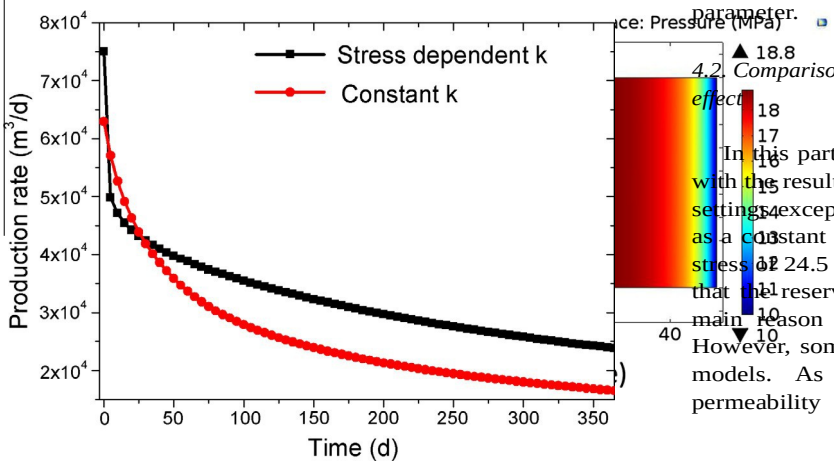

initial production rate of the constant permeability model is lower than the model that considers the per- meability change effect. This is caused by the fact that the constant rock matrix permeability is lower than that in the stress dependent permeability model at high reservoir pressure or low effective stress range. The more severe production rate decrease is caused by the rapid decrease in permeability near the flow out boundaries for the stress dependent permeability model.

The different production rate decline trends shown in Fig. 6 sug- gest that the stress dependent permeability plays a non-negligible part in the production rate calculation. As a result, the geomechan- ical effect should be carefully included in the shale gas well production prediction models. More accurate knowledge of the geomechanical effects may help in the optimization of shale gas well production strategies.

Fig. 6. Comparison of shale gas production rate in one year.

5. Conclusion

In this paper, the influence of geomechanical effects on the prediction of shale gas production rate decline is studied. Specifically, TPHM-based permeability–effective stress relationship is developed and incorporated into a simplified numerical model. The COMSOL is employed to calculate the reservoir pressure and production rate that evolve with time. As calculated, the reservoir pressure in the middle of the model decreases slowly with time and remains considerably higher than the well pressure even after 10-year production. The production rate curve showed a rapid decline trend in the initial stage and a long tail in the later stage. Moreover, the model considering the stress dependent permeability effect shows a much more rapid production rate decline trend in the initial stage than the model which set the permeability as a constant. The comparison result suggests that this geomechanical effect should be included in shale gas production prediction to ensure a better accuracy.

Acknowledgements

The authors are grateful to the National Natural Science Foundation of China (Grant No. 51374213), the National Natural Science Funds for Distinguished Young Scholars of China (Grant No. 51125017), the 2014 Innovative Team Project of Jiangsu Province of China and the Science Fund for Creative Research Groups of the National Natural Science Foundation of China (Grant No. 51421003) for the financial supports. Hui-Hai Liu also would like to thank the management of Aramco Research Center (Houston) for its approval to publish this work. We appreciate Dr. Jia-Jyun Dong from National Central University, Taiwan, for kindly provid- ing their data sets used in Figs. 1 and 2 of this paper. The authors would also like to express their gratitude to the editors and the anonymous reviewers for their valuable comments, which have greatly improved this paper.

References

[1] Cipolla CL, Lolon EP, Erdle JC, Rubin B. Reservoir modeling in shale-gas reservoirs. In: SPE eastern regional meeting, Charleston (WV, United States), 2009. http://dx.doi.org/10.2118/125530-MS.

[2] Jackson RB, Vengosh A, Carey JW, Davies RJ, Darrah TH, O'Sullivan F, et al. The environmental costs and benefits of fracking. Annu Rev Environ Resour 2014;39:327–62. http://dx.doi.org/10.1146/annurev-environ-031113-144051.

[3] Baihly J, Altman R, Malpani R, Luo F. Shale gas production decline trend comparison over time and basins. In: SPE annual technical conference and exhibition, Florence (Italy), 2010. http://dx.doi.org/10.2118/135555-MS.

[4] Arps JJ. Analysis of decline curves. SPE J 1945;160(1):228–47. http://dx.doi.org/10.2118/945228-g.

[5] Ilk D, Rushing JA, Perego AD. Exponential vs. hyperbolic decline in tight gas sands – understanding the origin and implications for reserve estimates using Arps' decline curves. In: SPE annual technical conference and exhibition, Denver (CO, United States), 2008. http://dx.doi.org/10.2118/116731-MS.

[6] Fetkovich MJ. Decline curve analysis using type curves. J Petrol Technol 1980;32(6):1065–77. http://dx.doi.org/10.2118/4629-PA.

[7] Fetkovich MJ, Bradley MD, Works AM, Thrasher TS. Depletion performance of layered reservoirs without crossflow. SPE Format Eval 1990;5(3):310–8. http://dx.doi.org/10.2118/18266-PA.

[8] Javadpour F, Fisher D, Unsworth M. Nanoscale gas flow in shale gas sediments. J Can Petrol Technol 2007;46(10):55–61. http://dx.doi.org/10.2118/07-10-06.

[9] Javadpour F. Nanopores and apparent permeability of gas flow in mudrocks (shales and siltstone). J Can Petrol Technol 2009;48(8):16–21. http://dx.doi.org/10.2118/09-08-16-da.

[10] Shabro V, Torres-Verdin C, Javadpour F. Numerical simulation of shale-gas production: from pore-scale modeling of slip-flow, Knudsen diffusion, and Langmuir desorption to reservoir modeling of compressible fluid. In: SPE North American unconventional gas conference and exhibition, The Woodlands (Texas), 2011. http://dx.doi.org/10.2118/144355-MS.

[11] Blasingame TA. The characteristic flow behavior of low-permeability reservoir systems. In: Unconventional reservoirs conference keystone, CO (United States), 2008. http://dx.doi.org/10.2118/114168-MS.

[12] Sun H, Chawathe A, Hoteit H, Shi X, Li L. Understanding shale gas flow behavior using numerical simulation. SPE J 2015;20(1):142–54. http://dx.doi.org/10.2118/167753-pa.

[13] Wang Z, Guo Y, Wang M. Permeability of high-Kn real gas flow in shale and production prediction by pore-scale modeling. J Nat Gas Sci Eng 2015;28:328–37. http://dx.doi.org/10.1016/j.jngse.2015.11.049.

[14] Wang C. Pressure transient analysis of fractured wells in shale reservoirs. Colorado School of Mines; 2013.
[15] Jin Z, Firoozabadi A. Effect of water on methane and carbon dioxide sorption in clay minerals by Monte Carlo simulations. Fluid Phase Equilibr 2014;38:210–20. http://dx.doi.org/10.1016/j.fluid.2014.07.035.
[16] Huang X, Bandilla KW, Celia MA. Multi-physics pore-network modeling of two-phase shale matrix flows. Transp Porous Med 2015;111(1):1–19. http://dx.doi.org/10.1007/s11242-015-0584-8.
[17] Cheng Y. Impact of water dynamics in fractures on the performance of hydraulically fractured wells in gas shale reservoirs. J Can Petrol Technol 2012;51(2):143–51. http://dx.doi.org/10.2118/127863-pa.
[18] Akkutlu IY, Fathi E. Multiscale gas transport in shales with local kerogen heterogeneities. In: SPE annual technical conference and exhibition, Denver (USA), 2012. http://dx.doi.org/10.2118/146422-pa.
[19] Ozkan E, Brown M, Raghavan R, Kazemi H. Comparison of fractured- horizontal-well performance in tight sand and shale reservoirs. SPE Reserv Eval Eng 2011;14(2):248–59. http://dx.doi.org/10.2118/121290-PA.
[20] Ozkan E, Raghavan RS, Apaydin OG. Modeling of fluid transfer from shale matrix to fracture network. In: SPE annual technical conference and exhibition, Florence (Italy), 2010. http://dx.doi.org/10.2118/134830-MS.
[21] Cao P, Liu J, Leong Y-K. A fully coupled multiscale shale deformation-gas transport model for the evaluation of shale gas extraction. Fuel 2016;178:103–17. http://dx.doi.org/10.1016/j.fuel.2016.03.055.
[22] Li X, Feng Z, Han G, Elsworth D, Marone C, Saffer D, et al. Breakdown pressure and fracture surface morphology of hydraulic fracturing in shale with H_2O, CO_2 and N_2. Geomech Geophys Geo-Energy Geo-Resour 2016;2(2):63–76. http://dx.doi.org/10.1007/s40948-016-0022-6.
[23] Middleton RS, Carey JW, Currier RP, Hyman JD, Kang Q, Karra S, et al. Shale gas and non-aqueous fracturing fluids: opportunities and challenges for supercritical CO_2. Appl Energ 2015;147:500–9. http://dx.doi.org/10.1016/j.apenergy.2015.03.023.
[24] Fakcharoenphol P, Charoenwongsa S, Kazemi H, Wu YS. The effect of water- induced stress to enhance hydrocarbon recovery in shale reservoirs. SPE J 2013;18(5):897–909. http://dx.doi.org/10.2118/158053-pa.
[25] Cho Y, Apaydin OG, Ozkan E. Pressure-dependent natural-fracture permeability in shale and its effect on shale-gas well production. In: SPE annual technical conference and exhibition, San Antonio (TX, United States), 2012. http://dx.doi.org/10.2118/159801-MS.
[26] Baz˘ant ZP, Salviato M, Chau VT, Visnawathan H, Zubelewicz A. Why fracking works. J Appl Mech 2014;81(10):101010. http://dx.doi.org/10.1115/1.4028192.
[27] Gan Q, Elsworth D. A continuum model for coupled stress and fluid flow in discrete fracture networks. Geomech Geophys Geo-Energy Geo-Resour 2016;2(1):43–61. http://dx.doi.org/10.1007/s40948-015-0020-0.
[28] Gensterblum Y, Ghanizadeh A, Cuss RJ, Amann-Hildenbrand A, Krooss BM, Clarkson CR, et al. Gas transport and storage capacity in shale gas reservoirs – a review. Part A: Transport processes. J Unconv Oil Gas Resour 2015;12:87–122. http://dx.doi.org/10.1016/j.juogr.2015.08.001.
[29] Ghanizadeh A, Gasparik M, Amann-Hildenbrand A, Gensterblum Y, Krooss B M. Experimental study of fluid transport processes in the matrix system of the European organic-rich shales: I. Scandinavian. Mar Petrol Geol 2014;51:79–99. http://dx.doi.org/10.1016/j.marpetgeo.2013.10.013.
[30] Heller R, Vermylen J, Zoback M. Experimental investigation of matrix permeability of gas shales. AAPG Bull 2014;98(5):975–95. http://dx.doi.org/10.1306/09231313023.
[31] Dong J-J, Hsu J-Y, Wu W-J, Shimamoto T, Hung J-H, Yeh E-C, et al. Stress-dependence of the permeability and porosity of sandstone and shale from TCDP Hole-A. Int J Rock Mech Min Sci 2010;47(7):1141–57. http://dx.doi.org/10.1016/j.ijrmms.2010.06.019.
[32] Kwon O, Kronenberg AK, Gangi AF, Johnson B. Permeability of Wilcox shale and its effective pressure law. J Geophys Res Sol Earth 2001;106(B9):19339–53. http://dx.doi.org/10.1029/2001jb000273.
[33] Metwally YM, Sondergeld CH. Measuring low permeabilities of gas-sands and shales using a pressure transmission technique. Int J Rock Mech Min Sci 2011;48(7):1135–44. http://dx.doi.org/10.1016/j.ijrmms.2011.08.004.
[34] Tinni A, Fathi E, Agarwal R, Sondergeld CH, Akkutlu IY, Rai CS. Shale permeability measurements on plugs and crushed samples. In: SPE Canadian unconventional resources conference, Calgary (Alberta, Canada), 2012. http://dx.doi.org/10.2118/162235-MS.
[35] Dewhurst DN, Aplin AC, Sarda JP, Yang YL. Compaction-driven evolution of porosity and permeability in natural mudstones: an experimental study. J Geophys Res Sol Earth 1998;103(B1):651–61. http://dx.doi.org/10.1029/97JB02540.
[36] Zheng J, Zheng L, Liu H-H, Ju Y. Relationships between permeability, porosity and effective stress for low-permeability sedimentary rock. Int J Rock Mech Min Sci 2015;78:304–18. http://dx.doi.org/10.1016/j.ijrmms..04.025.
[37] Li N, Ran Q, Li J, Yuan J, Wang C, Wu Y-S. A multiple-continuum model for simulation of gas production from shale gas reservoirs. In: SPE reservoir characterisation and simulation conference and exhibition, Abu Dhabi (United Arab Emirates), 2013. http://dx.doi.org/10.2118/165991-MS.
[38] Davies J, Davies D. Stress-dependent permeability: characterization and modeling. Soc Petrol Eng J 2001;6(02):224–35. http://dx.doi.org/10.2118/71750-PA.
[39] Rutqvist J, Wu YS, Tsang CF, Bodvarsson G. A modeling approach for analysis of coupled multiphase fluid flow, heat transfer, and deformation in fractured porous rock. Int J Rock Mech Min Sci 2002;39(4):429–42. http://dx.doi.org/10.1016/S1365-1609(02)00022-9.
[40] Yu Z, Lerche I. Modelling abnormal pressure development in sandstone/shale basins. Mar Petrol Geol 1996;13(2):179–93. http://dx.doi.org/10.1016/0264-8172(95)00036-4.
[41] Guo XW, He S, Liu KY, Song GQ, Wang XJ, Shi ZS. Oil generation as the dominant overpressure mechanism in the Cenozoic Dongying depression, Bohai Bay Basin, China. AAPG Bull 2010;94(12):1859–81. http://dx.doi.org/10.1306/05191009179.
[42] Yang F, Ning Z, Wang Q, Liu H. Pore structure of Cambrian shales from the Sichuan Basin in China and implications to gas storage. Mar Petrol Geol 2016;70:14–26. http://dx.doi.org/10.1016/j.marpetgeo.2015.11.001.
[43] Al-Wardy W, Zimmerman RW. Effective stress law for the permeability of clay-rich sandstones. J Geophys Res Sol Earth 2004;109(B4). http://dx.doi.org/10.1029/2003JB00283.
[44] Ghabezloo S, Sulem J, Guédon S, Martineau F. Effective stress law for the permeability of a limestone. Int J Rock Mech Min Sci 2009;46(2):297–306. http://dx.doi.org/10.1016/j.ijrmms.2008.05.006.
[45] Liu H-H, Wei M-Y, Rutqvist J. Normal-stress dependence of fracture hydraulic properties including two-phase flow properties. Hydrogeol J 2013;21(2):371–82. http://dx.doi.org/10.1007/s10040-012-0915-6.
[46] Liu H-H, Rutqvist J, Berryman JG. On the relationship between stress and elastic strain for porous and fractured rock. Int J Rock Mech Min Sci 2009;46(2):289–96. http://dx.doi.org/10.1016/j.ijrmms.2008.04.005.
[47] Zhao Y, Liu H-H. An elastic stress–strain relationship for porous rock under anisotropic stress conditions. Rock Mech Rock Eng 2012;45(3):389–99. http://dx.doi.org/10.1007/s00603-011-0193-y.
[48] Liu HH, Rutqvist J, Birkholzer JT. Constitutive relationships for elastic deformation of clay rock: data analysis. Rock Mech Rock Eng 2011;44(4):463–8. http://dx.doi.org/10.1007/s00603-010-0131-4.
[49] Loucks RG, Reed RM, Ruppel SC, Hammes U. Spectrum of pore types and networks in mudrocks and a descriptive classification for matrix-related mudrock pores. AAPG Bull 2012;96(6):1071–98. http://dx.doi.org/10.1306/08171111061.
[50] Jaeger JC, Cook NG, Zimmerman R. Fundamentals of rock mechanics. Malden (MA, USA): Wiley-Blackwell; 2007.
[51] Sisavath S, Jing XD, Zimmerman RW. Effect of stress on the hydraulic conductivity of rock pores. Phys Chem Earth Pt A: Solid Earth Geodesy 2000;25(2):163–8. http://dx.doi.org/10.1016/S1464-1895(00)00026-0.
[52] Sisavath S, Jing XD, Zimmerman RW. Laminar flow through irregularly-shaped pores in sedimentary rocks. Transp Porous Med 2001;45(1):41–62. http://dx.doi.org/10.1023/a:1011898612442.
[53] Sisavath S, Al-Yaarubi A, Pain CC, Zimmerman RW. A simple model for deviations from the cubic law for a fracture undergoing dilation or closure. Pure Appl Geophys 2003;160(5–6):1009–22. http://dx.doi.org/10.1007/pl00012558.
[54] Kilmer NH, Morrow NR, Pitman JK. Pressure sensitivity of low permeability sandstones. J Petrol Sci Eng 1987;1(1):65–81. http://dx.doi.org/10.1016/0920-4105(87)90015-5.
[55] Brower K, Morrow N. Fluid flow in cracks as related to low-permeability gas sands. Soc Petrol Eng J 1985;25(2):191–201. http://dx.doi.org/10.2118/11623-PA.
[56] Smith TM, Sayers CM, Sondergeld CH. Rock properties in low-porosity/low-permeability sandstones. Lead Edge 2009;28(1):48–59. http://dx.doi.org/10.1190/1.3064146.
[57] Spencer CW. Review of characteristics of low-permeability gas reservoirs in western United States. AAPG Bull 1989;73(5):613–29. http://dx.doi.org/10.1306/44b4a23a-170a-11d7-8645000102c1865d.
[58] Byrnes AP, Castle JW. Comparison of core petrophysical properties between low-permeability sandstone reservoirs: Eastern US Medina group and Western US Mesaverde group and Frontier formation. In: SPE rocky mountain regional/ low-permeability reservoirs symposium and exhibition, Denver (Colorado, USA), 2000. http://dx.doi.org/10.2118/60304-MS.
[59] Witherspoon PA, Wang JSY, Iwai K, Gale JE. Validity of cubic law for fluid flow in a deformable rock fracture. Water Resour Res 1980;16(6):1016–24. http://dx.doi.org/10.1029/WR016i006p01016.
[60] Zimmerman R, Bodvarsson G. Hydraulic conductivity of rock fractures. Transp Porous Med 1996;23(1):1–30. http://dx.doi.org/10.2172/60784.

$$Q(t) = \frac{Q_i}{[1 + bDt]^{1/b}}$$

$$\phi = \phi_{e,0}(1 - C_e\sigma) + \gamma_t \exp\left(-\frac{\sigma}{K_t}\right)$$

$$\phi_e = \phi_{e,0}(1 - C_e\sigma)$$

$$\phi_t = \gamma_t \exp\left(-\frac{\sigma}{K_t}\right)$$

$$k_e = k_{e,0}\exp\left[\beta(\phi_e - \phi_{e,0})\right] = k_{e,0}\exp\left[-\beta C_e \phi_{e,0}\sigma\right]$$

$$k_t = \alpha\phi_t^m = \alpha\left[\gamma_t \exp\left(-\frac{\sigma}{K_t}\right)\right]^m$$

$$k = k_{e,0}\exp\left[-\beta C_e \phi_{e,0}\sigma\right] + \alpha\left[\gamma_t \exp\left(-\frac{\sigma}{K_t}\right)\right]^m$$

Table 1
Input parameters for shale gas production simulation.

Viscosity (Pa·s)	1.12×10^{-5}
Permeability (m^2)	$k = k_{e,0}\exp\left[-\beta C_e \phi_e\right.$
$k_{e,0}$ (m^2)	10^{-20}
$\beta C_e \phi_{e,0}$ (MPa^{-1})	0.01
α (m^2)	10^{-16}
γ_t	0.005
K_t (MPa)	8.00
m	3.00
Initial pore pressure (MPa)	30.00
Confining pressure (MPa)	34.50
Production well pressure (MPa)	10.00